

Effect and Compensation of Timing Jitter in Through-Wall Human Indication via Impulse Through-Wall Radar

Guofu ZHU, Jun HU, Tian JIN, Zhimin ZHOU

College of Electronic Science and Engineering, National University of Defense Technology, Changsha, P. R. China

zhuguofu@nudt.edu.cn, hujunnudt@yahoo.com, tianjin@nudt.edu.cn, zhouzhimin@nudt.edu.cn

Abstract. *Impulse through-wall radar (TWR) is considered as one of preferred choices for through-wall human indication due to its good penetration and high range resolution. Large bandwidth available for impulse TWR results in high range resolution, but also brings an atypical adversity issue not substantial in narrowband radars — high timing jitter effect, caused by the non-ideal sampling clock at the receiver. The fact that impulse TWR employs very narrow pulses makes little jitter inaccuracy large enough to destroy the signal correlation property and then degrade clutter suppression performance. In this paper, we focus on the timing jitter impact on clutter suppression in through-wall human indication via impulse TWR. We setup a simple timing jitter model and propose a criterion namely average range profile (ARP) contrast to evaluate the jitter level. To combat timing jitter, we also develop an effective compensation method based on local ARP contrast maximization. The proposed method can be implemented pulse by pulse followed by exponential average background subtraction algorithm to mitigate clutters. Through-wall experiments demonstrate that the proposed method can dramatically improve through-wall human indication performance.*

Keywords

Through-wall radar, human target indication, clutter suppression, timing jitter, average range profile, local contrast maximization.

1. Introduction

Through-wall human indication is of great interest in homeland security and disaster rescue applications [1]. Ultra-wideband (UWB) through-wall radar (TWR) has emerged as a promising technique due to its high range resolution and good penetration. Impulse TWR is one of the preferred choices, which generally employs extremely narrow pulse (typically few nanoseconds) to provide large bandwidth for high range resolution.

However, through-wall human indication with UWB TWR is faced with many challenges arising from both the sensing scenario and the radar system. Low reflectivity of

human body, strong interference including antenna cross-talk, and clutters from walls, furniture, etc., and high signal attenuation of walls [2] result in extremely low signal-to-clutter ratio (SCR), which makes clutter suppression play a key role in through-wall human indication. In the past few years, many effective methods operating in time domain [3]-[9] or frequency domain [10]-[11] have been developed to obtain high clutter suppression performance, based on the fact that there are always motions in live people, e.g. heart-beating and respiration in stationary people, limbs or torso motions in moving people, etc.

Time-domain clutter suppression methods such as background subtraction [6], moving target indication (MTI) [8], moving target detection (MTD) filter [9], etc. succeed in indicating human targets based on the assumption that static clutter signals are time invariant. Frequency-domain methods reported in [11], [12] to detect trapped people divide clutters into static and unstatic parts to remove, and the jitter distortions are treated as unstatic clutters. Both of the two methods adopt linear trend subtraction (LTS) to mitigate the static components. As to the unstatic components, reference [11] decomposes the range-frequency matrix by means of single value decomposition (SVD) into different subspaces and removes the unstatic clutter subspace empirically, while reference [12] uses an improved automatic approach based on constant false alarm ratio (CFAR) and clustering to remove the unstatic components. However, neither of the above two references have examined the timing jitter effect on clutter suppression in detail. Besides, their methods are complicated.

Note that whether operating in the time domain or frequency domain, clutter suppression requires a steady correlation between received pulses. However, it is difficult to satisfy the steady correlation with the presence of system instability in real impulse systems. One issue is introduced by the non-ideal sampling clock at receiver, which in effect gives room for sampling offsets referred to as timing jitter [13]. Typically, timing jitter ranges in 10-150 ps in impulse systems [14], but the fact that impulse TWR employs nanosecond-short pulses makes the sensitivity to timing jitter significant, and even common jitter inaccuracy is large enough to degrade the signal correlation [13], [15]. As a result, echoes from stationary scatterer including antenna cross-talk, wall clutters, etc. time varying both in amplitude

and delay (in this study, we concern impulse TWR with two co-located antennas which keeps immobile when working and the antenna cross-talk can also be treated as clutters from a stationary scatterer in close range). Compared with the weak echoes of human body, these clutters are so strong that even few residuals because of jitter distortion are large enough to cause false alarms. In frequency domain, timing jitter distortion covers the heart-beating and respiration frequency band and makes it difficult to extract these components.

In order to analyze the impact of timing jitter on clutter suppression, firstly, we setup a simple model, and propose a criterion namely average range profile (ARP) contrast to evaluate the jitter level. Contrast is usually adopted to measure the sharpness of an image. Here, lower jitter level will yield a sharper ARP, whose contrast is higher. Then, a range alignment method based on local ARP contrast maximization is introduced to eliminate the timing jitter effect. Correlation based range alignment method [16] was introduced to combat timing jitter effect in coupling suppression [17] and clutter mitigation [18], but it is widely accepted that this method is somewhat sensitive to noise. Additionally, it has the defect of misalignment error accumulation. By contrast, the range alignment method based on local ARP contrast maximization is immune from the above defects, and it is proved that this method is essentially an extension of the maximum correlation range alignment technique. Finally, an effective time-domain method — exponential average background subtraction (EABS) [6] is applied to remove clutters. Since EABS weights previous pulses by exponential coefficients to estimate the background data, it permits meaningful control over its clutter-reduction behavior and can achieve good results in clutter suppression [6], [19].

The paper is organized as follows. Section 2 gives a brief description of our impulse TWR and the experimental scenario. Section 3 setups a model of timing jitter, presents some simulation results and analysis. Section 4 describes in detail the introduced method to compensate timing jitters, followed by clutter suppression to achieve target indication. Various through-wall experiments are provided and discussed in Section 5. Conclusion is drawn in Section 6.

2. Radar System

We have developed a portable real-time mono-static 1-D time-domain impulse TWR [20] with two co-located Archimedean spiral antennas, consisting of antenna module, transmitting and receiving module, and data acquiring, processing and displaying module, as shown in Fig. 1. Transmitting and receiving are controlled by frequency synthesizer and timing controller (FSTC). As Fig. 2a) shows, the TWR transmits about 2 ns width first-order Gaussian pulses with 20 Hz pulse repetition frequency (PRF). At the receiver, the sampling rate is 8 GHz. The impulse TWR remains immobile and the recorded pulses

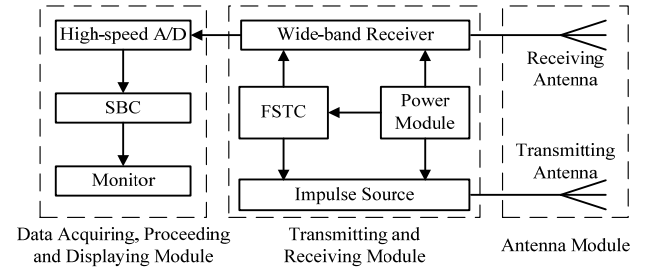


Fig. 1. Block diagram of the impulse TWR.

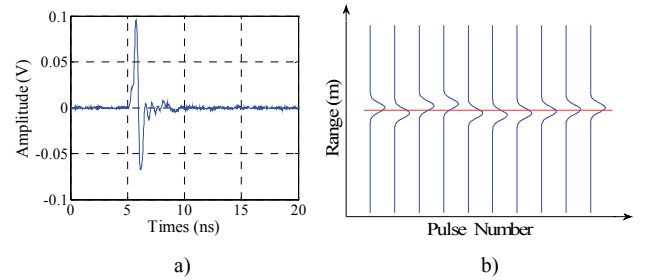


Fig. 2. a) Transmitting waveform; b) data matrix.

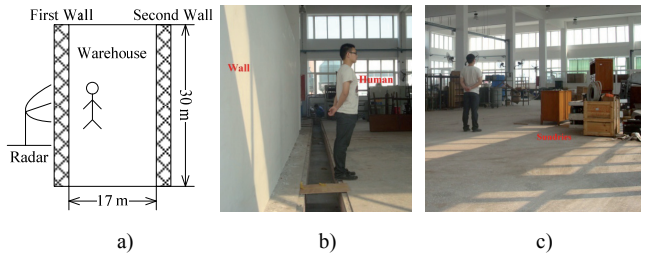


Fig. 3. a) Arrangements and b), c) photos of the scenario.

are aligned to each other creating a 2D matrix, in which the fast-time dimension is related to echo time delay corresponding to measured range, while the slow-time dimension is related to pulse number, as shown in Fig. 2b).

With the TWR, we have conducted through-wall experiments, focusing on the scenario that human targets locate behind wall with all the other objects in their surroundings static as delineated in Fig. 3. The wall to penetrate is a 30 cm thick brick wall of a $30 \times 17 \text{ m}^2$ warehouse, and there are a pile of sundries including cabinets, cables, metal shelves, etc. lying in the range of 3-6 m away from the wall as shown in Fig. 3b).

3. Timing Jitter Analysis

3.1 Model Description

Let the first-order Gaussian function denote the transmitting waveform

$$p_t(t) = -\frac{At}{\sigma_t^2} \exp\left\{-\frac{t^2}{2\sigma_t^2}\right\} \quad (1)$$

where A is an amplitude normalization constant, σ_t is related to the pulse width. Smaller σ_t results in narrower

pulse. Consider the propagation delay τ encountered by the signal as it travels from the transmitter to a scatterer behind wall and back to the receiver, ignore the propagation attenuation and wall effect, and let $p_r(t)$ denote the received analog time continuous echo signal. Due to the differential characteristic of the antennas [21], the received signal $p_r(t)$ can be modeled as five-order Gaussian function

$$p_r(t) = \frac{A(\tau-t)}{\sigma_t^6} \left[\left(\frac{\tau-t}{\sigma_t} \right)^4 - 10 \left(\frac{\tau-t}{\sigma_t} \right)^2 + 15 \right] \exp \left\{ -\frac{(\tau-t)^2}{2\sigma_t^2} \right\}. \quad (2)$$

Ideally, the received echo signals from stationary scatterers at different measured time are time-invariant. For simplicity, we assume that the noise signal added on measurement is also changeless, and far less than the scatterer echo signals. At the receiver, let T_s denote the sampling period and $n_r(t)$ denote the noise signal. Due to the presence of jitter ε on the sampling clock, the m th ideal sample at time $t_m = mT_s$ will be taken at $mT_s + \varepsilon(n)$

$$\begin{aligned} p_s(t_m, n) &= p_r(t_m) + n_r(t_m) \\ &= p_r(mT_s + \varepsilon(n)) + n_r(mT_s + \varepsilon(n)) \end{aligned} \quad (3)$$

where $\varepsilon(n)$ denotes the timing jitter in the n th measurement. Timing jitter because of the non-ideal sampling clock is usually considered as a time varying random process independent from the analog time continuous input signal $p_r(t)$, which means jitter at each sample in a single measurement is different. But in this study we simply assume that all samples in a specified measurement suffer from the same jitter level.

Expanding (3) using Taylor series around t_m and ignoring the high-order items, we obtain the approximation of (3)

$$p_s(t_m, n) \approx p_r(t_m) + n_r(t_m) + \left. \frac{\partial p_r(t)}{\partial t} \right|_{t=t_m} \varepsilon(n) + \left. \frac{\partial n_r(t)}{\partial t} \right|_{t=t_m} \varepsilon(n) \quad (4)$$

where the fourth item is the interaction of timing jitter $\varepsilon(n)$ and noise $n_r(t)$ and can be ignored under high signal-to-noise ratio (SNR) [22].

As the effect of the sampling instant uncertainty is concerned, we neglect the quantization error. Let $k(t) = \partial p_r(t) / \partial t$ denote the first-order derivative of $p_r(t)$, then the discrete signal corresponding to $p_s(t_m, n)$ is

$$p(m, n) = p_r(m) + n_r(m) + k(t_m) \varepsilon(n). \quad (5)$$

In general, timing jitter ε is modeled as a time discrete Gaussian random process with time step T_p namely pulse repetition interval (PRI), having mean $\mu_J = 0$ [23]

$$\varepsilon(n) \sim N(0, \sigma_J^2) \quad (6)$$

where σ_J is the standard variation, typically ranging in 10-150 ps in UWB receivers [14], and $N(\mu, \sigma^2)$ denotes the Gaussian random process. Thus, in the slow-time dimension, for a specified rang cell m , $p(m, n)$ also obeys a discrete Gaussian random process with time step T_p , having mean $\mu_p = p_r(m) + n_r(m)$ and variation $\sigma_p^2 = |k(t_m)| \sigma_J^2$, i.e.

$$p(m, n) \sim N(p_r(m) + n_r(m), |k(t_m)| \sigma_J^2). \quad (7)$$

Obviously, because of the presence of the distortion, $p(m, n)$ randomly fluctuates around its mean μ_p , depending on the first-order derivative $k(t)$ at t_m . In other words, the distribution of $p(m, n)$ is related to the change rate of $p_r(t)$. Nevertheless, the transmitting pulse is very narrow, and thus the received signal $p_r(t)$ has a great change rate, which finally enlarges the timing jitter distortion.

3.2 Effect of Timing Jitter

Ignoring the noise signal $n_r(t)$, simulations of echoes of a stationary scatterer in range 1.2 m under timing jitters with different σ_J are performed. The detailed simulation parameters are listed in Tab. 1. Fig. 4a) shows the normalized power spectrum density (PSD) of $p(m, n)$ under the timing jitter with $\sigma_J = 80$ ps. The shadow region represents the frequency band ranging in 0.2-1 Hz corresponding to heart-beating, respiration, arm swigging and so on. Fig. 4c) shows the corresponding range-frequency matrix without zero-frequency components. The timing jitter distortion occupies the entire frequency band, making it difficult for frequency-methods to correctly extract the frequency components of stationary people from clutters, without compensating distortion.

Parameter	Pulse Width	t_0	$1/T_s$	τ	PRF	M	N
Value	2.0 ns	0 s	8 GHz	8 ns	20 Hz	160	200

Tab. 1. Simulation parameters.

Fig. 4b) plots the corresponding rang profiles, and obviously nonlinear drift occurs. Fig. 4d) displays the clutter suppression result by EABS. Obviously, with the presence of timing jitter, residual clutters are still considerable. It is also difficult for time-domain methods to distinguish the weak echoes of human target from the residual clutters, which means that false alarms could occur.

Timing jitter exerts a significant effect on clutter suppression in impulse TWR. We introduce a criterion namely ARP contrast to evaluate the jitter level. Contrast is usually adopted to measure the sharpness of an image. The sharper an image is, the larger its contrast is. Here, define the ARP of N sampled pulses with timing jitter as

$$s(m, \boldsymbol{\varepsilon}) = \sum_{n=1}^N p(m, n) \quad (8)$$

where $\boldsymbol{\varepsilon} = [\varepsilon(1), \varepsilon(2), \dots, \varepsilon(N)]$ is the timing jitter vector, and the contrast of s is defined as

$$C = \frac{\sigma[s]}{E[s]} = \sqrt{\frac{1}{M} \sum_{m=1}^M s^2 - (E[s])^2} / E[s] \quad (9)$$

where $E[s]$ and $\sigma[s]$ denote the mean and standard deviation of s respectively and M represents the pulse length. For N measured pulses of a stationary scatterer, the ideal different measured echo signals are changeless. The larger timing jitter is, the more the misalignment of range profiles will be and the smaller the ARP contrast will be.

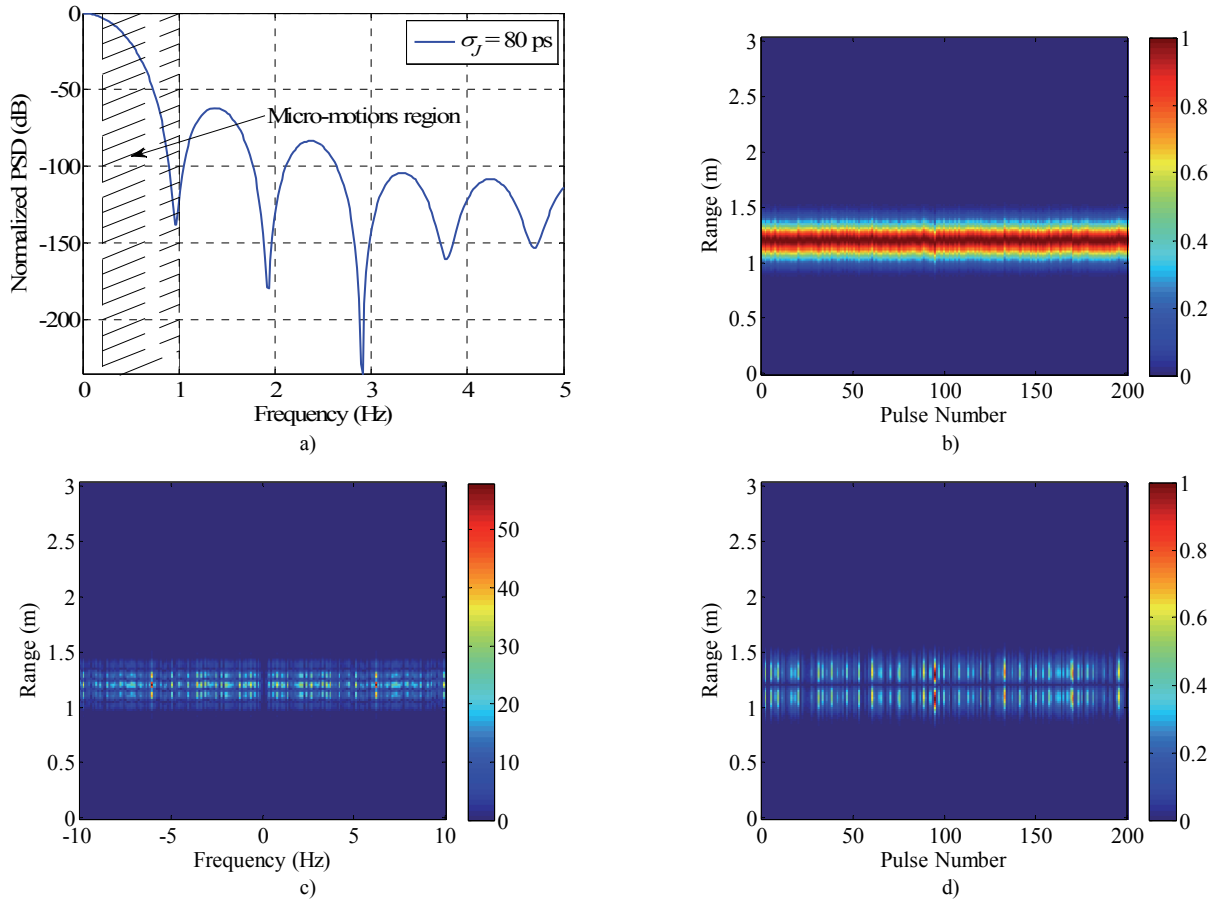


Fig. 4. Simulation results of received echo under timing jitter with $\sigma_j = 50$ ns. a) Distribution of pulse peak value and peak index; b) range profiles; c) range-frequency matrix without zero frequency components; d) EABS processing result.

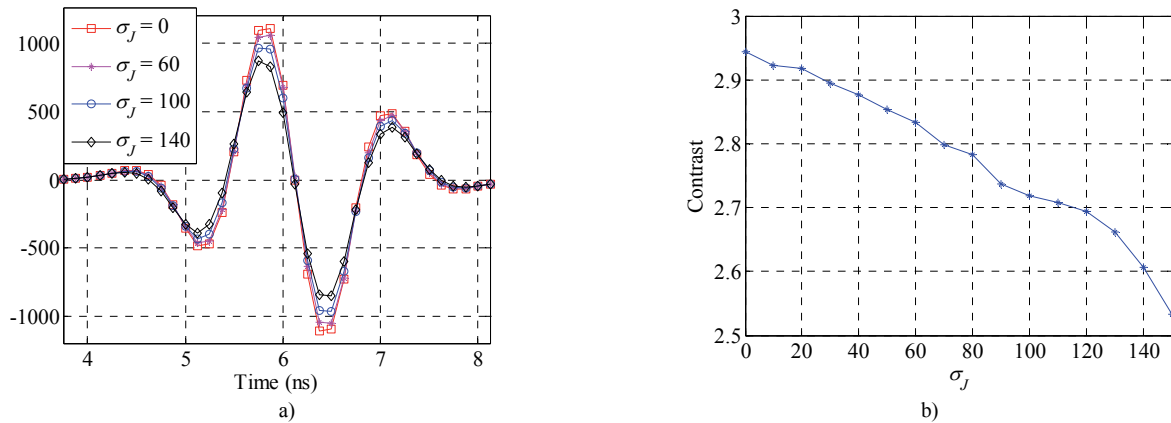


Fig. 5. Distributions of (a) ARP and (b) ARP contrast under timing jitters with different σ_j .

Some simulated results about the distributions of ARP and ARP contrasts under timing jitter with different σ_j are plotted in Fig. 5. As Fig. 5a) shows, without timing jitter namely $\sigma_j = 0$, the ARP distribution is the sharpest. With the increase of σ_j , the ARP sharpness decreases. As Fig. 5b) shows, the smaller σ_j is, the larger its contrast is. ARP contrast decreases monotonously with the timing jitter level σ_j . Thus, ARP contrast is able to describe the timing jitter level of N measured pulses, and furthermore it can be employed to evaluate the jitter compensation.

4. Target Indication

Both of the amplitude and delay of received pulses are distorted by timing jitters and should be compensated. As Fig. 6 shows, firstly interpolation along the fast-time is implemented to recover timing jitters, which can make compensation reach the sub-range level.

4.1 Timing Jitter Compensation

Amplitude compensation is completed simply by nor-

malizing each pulse along the fast-time dimension, i.e.

$$p_a(m, n) = p(m, n) / \max_m \{p(m, n)\}. \quad (10)$$

As discussed in Section 3, our delay compensation method is designed to maximize the local ARP contrast. Let $\mathbf{W}_a = [p_a(n-N+1), p_a(n-N+2), \dots, p_a(n)]$ stand for the sliding window matrix, and $\Delta \mathbf{r} = [\Delta r(1), \Delta r(2), \dots, \Delta r(N)]$ represent the range vector corresponding to the timing jitter vector $\boldsymbol{\varepsilon}$, where N is the sliding window width. For a given sliding window, the mean of its ARP $E[s(r, \Delta \mathbf{r})]$ is constant. Thus, the ARP contrast in (9) can be redefined as

$$C' = \int_r s^2(r, \Delta \mathbf{r}) dr. \quad (11)$$

The necessary condition for maximizing (11) is described by setting the derivate of C' with respect to $\Delta \mathbf{r}$ equal to zero

$$\frac{\partial C'}{\partial \Delta \mathbf{r}} = \int_r 2s(r, \Delta \mathbf{r}) \frac{\partial s(r, \Delta \mathbf{r})}{\partial \Delta \mathbf{r}} dr = 0. \quad (12)$$

Reformulate s in frequency domain

$$s(r, \Delta \mathbf{r}) = \int_{f_r} \left[\sum_{n=1}^N P_a(f_r, n) e^{j2\pi f_r \Delta r(n)} \right] e^{j2\pi f_r r} df_r \quad (13)$$

where $P_a(f_r, n)$ stands for the Fourier spectrum of $p_a(r, n)$ in the fast-time dimension. Substitute (13) into (12)

$$\int_r 2s(r, \Delta \mathbf{r}) \times \left(\int_{f_r} j2\pi f_r \left[\sum_{n=1}^N P_a(f_r, n) e^{j2\pi f_r \Delta r(n)} \right] e^{j2\pi f_r r} df_r \right) dr = 0 \quad (14)$$

Interchanging the order of integration, we obtain

$$\sum_{n=1}^N \int_{f_r} j4\pi f_r P_a(f_r, n) \left[\int_r s(r, \Delta \mathbf{r}) e^{j2\pi f_r r} dr \right] e^{j2\pi f_r \Delta r(n)} df_r = 0. \quad (15)$$

Note that the integral within the square brackets is the conjugated Fourier spectrum of $s(r, \Delta \mathbf{r})$ which is denoted as $S^*(f_r)$. Consequently, (15) can be rewritten as

$$\sum_{n=1}^N \int_{f_r} j4\pi \left[f_r P_a(f_r, n) S^*(f_r) \right] e^{j2\pi \Delta r(n) f_r} df_r = 0. \quad (16)$$

As per the differentiation property of the Fourier transform, we obtain

$$\sum_{n=1}^N \frac{\partial \left[p_a(\Delta r(n), n) \otimes s(-\Delta r(n)) \right]}{\partial \Delta r(n)} = 0 \quad (17)$$

where \otimes denotes the 1-D convolution. Solving (17) is equivalent to searching for $\Delta r(n)$ to satisfy

$$\frac{\partial \text{COR}(p_a(r, n), s(r))}{\partial r} \Big|_{r=\Delta r(n)} = 0, n = 1, 2, \dots, N \quad (18)$$

where $\text{COR}(p_a(r, n), s(r)) = p_a(r, n) \otimes s(-r)$ represents the cross correlation between $p_a(r, n)$ and $s(r)$, and $\Delta r(n)$ is the coordinate satisfying (18). The $\Delta \mathbf{r}$ to be compensated must consist of the component $\Delta r(n)$.

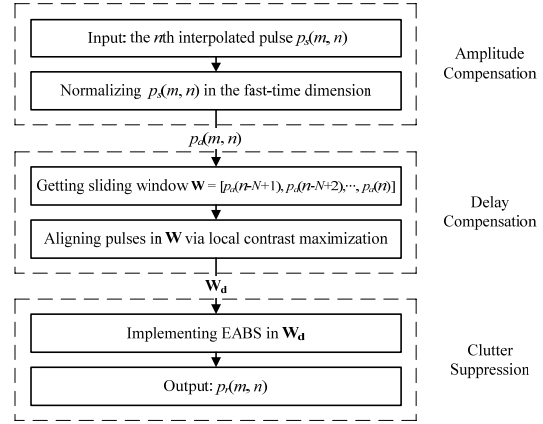


Fig. 6. Flow chart of the proposed approach.

The sequential search scheme developed in [24] is employed to search the optimum $\Delta \mathbf{r}$ in the sliding window. Let k be the iteration number and the initial value of $\Delta \mathbf{r}$ be zero. In the k th iteration, $\Delta \mathbf{r}$ is updated as follow

$$\Delta_r^k(n) = \Delta_r^{k-1}(n) + \arg \left\{ \max_r \left[p_a(r + \Delta_r^{k-1}(n), n) \otimes s^{k-1}(-r) \right] \right\} \quad (19)$$

where

$$s^{k-1}(r) = \sum_{i=n-N+1}^n p_a(r + \Delta_r^{k-1}(i), i). \quad (20)$$

For each trial, the ARP contrast of the sliding window is measured. The aforementioned processing steps are executed iteratively until the contrast stops increasing. The corresponding $\Delta \mathbf{r}$ is used to align the pulses in the sliding window to complete jitter delay compensation.

The optimization problem is of N dimension. Note that when the sliding window width N equals to 1, the local ARP contrast maximization algorithm becomes the maximum correlation method [16].

4.2 Clutter Suppression

As to clutter suppression, time-domain methods like background subtraction can be implemented pulse by pulse. In the background subtraction paradigms, background data is estimated first using previous pulses and then subtracted from the current pulse to indicate targets.

In the EABS [6], previous pulses are weighted by exponential coefficients to estimate the background data. Let $\mathbf{W}_a = [p_a(n-N+1), p_a(n-N+2), \dots, p_a(n)]$ denote the sliding window matrix after timing jitter compensation, EABS in \mathbf{W}_a can be described as

$$p_r(m, n) = p_d(m, n) - b(n) = p_d(m, n) - \sum_{i=1}^{N-1} \alpha^i p_d(m, n-i) \quad (21)$$

where $b(n)$ stands for the background and α is a constant weighting factor in the range $0 < \alpha < 1$. Compared with the two-pulse cancellation [8], EABS makes use of more his-

tory information. Compared with the accumulated average background subtraction (AABS) [6], EABS is more reasonable as exponential weighting coefficients gradually weaken the previous pulses effect with time increase.

As the weighting factor α increases, more low components will be reserved by EABS [19]. Generally the frequency corresponding to the respiration and heartbeat in stationary people ranges in 0.2-0.7 Hz. Thus in order to effectively indicate the stationary human targets, the weighting factor α of EABS is set to 0.95 in this paper.

5. Experimental Results

Using our impulse TWR, we have carried out various through-wall experiments on human targets in the scene described in Section 2. With different standoff distances between radar and wall, different people in different ranges are considered so that the influence of the timing jitter on clutter suppression could be determined. In the experiments, scatterer range represents the radial distance between scatterer and radar, and both the proposed method and EABS are employed to process the measured data. In

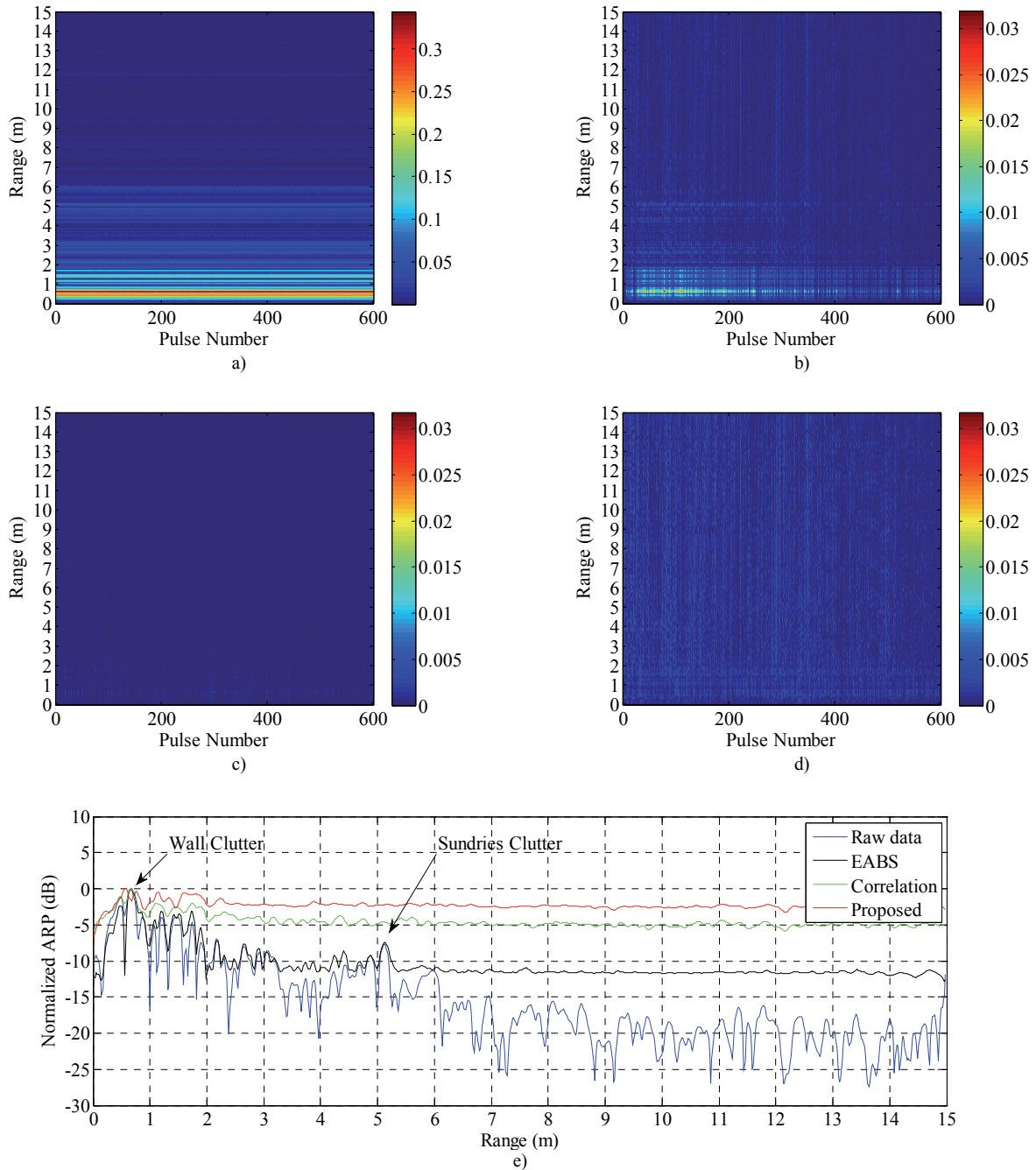


Fig. 7. Radar is placed close to wall to sense the empty scene: a) rang profiles of raw measured data; results of clutter suppression using b) EABS, c) correlation and d) the proposed method; e) normalized ARP distributions of raw data, and clutter suppression results using EABS and the proposed method.

the processing, the constant weighting factor α of EABS equals 0.95, and the sliding window width N in the proposed method is 15, and the wall effect on the speed of electromagnetic propagation is ignored. Thus, little deviation from the actual position of scatterers occurs in the experimental results

5.1 Measurement of Empty Scene

In the first case, the radar is placed close to wall to sense the experimental scene described in Fig. 3 without human targets behind the wall. Fig. 7a) shows the raw

measured range profiles of the empty scene, wall clutters cover the range of 0-2 m, the strongest echoes belonging to the wall clutters appear in range 0.5 m and the clutters backscattered from the pile of sundries occupy the range of around 5 m. Fig. 7b) shows the clutter suppression result using EABS. Residual wall clutters in the range of 0-2 m are clearly visible and residual sundries clutters are also visible in the range of around 5 m. As shown in Fig. 7c) and d), with timing jitter compensation, both the wall clutters and the sundries clutters are removed cleanly by the correlation and proposed method, respectively. Comparison of the four ARP distributions is delineated in Fig. 7e).

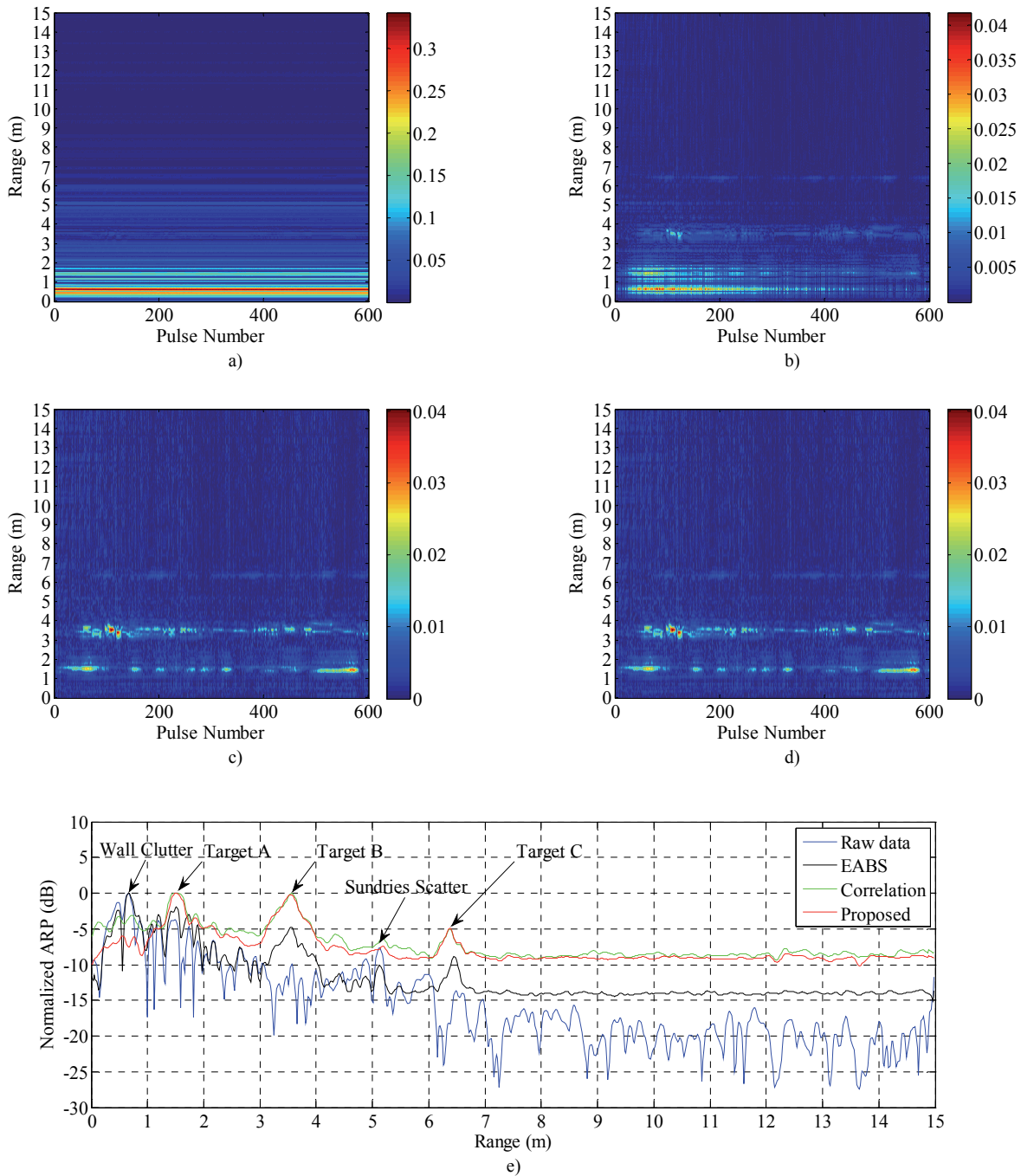


Fig. 8. The radar is placed close to wall to sense the scene with three human targets behind wall in different ranges. The organization of this figure is exactly the same as that of Fig. 7.

From the raw data ARP distribution, we can see that without clutter suppression echoes reach the strongest in the wall clutters range and gradually attenuate with the range increase. In the ARP distribution corresponding to EABS, the residual clutters are about 10 dB higher than the average level which are large enough to cause false alarms, and the residual sundries clutters are also 4 dB higher than the level of adjacent cell ranges. The much smoother ARP distributions of the correlation and proposed methods indicate that strong clutters are well mitigated. By comparison, the proposed method yields the smoothest curve with only little fluctuation around -3 dB, and further improves the clutter mitigation performance.

5.2 Radar Close to Wall

In the second case, the radar is placed close to wall, three people locate in the scene behind wall, and their activities are described in Tab. 2. Fig. 8a) shows the range profiles of the raw data. As same to the first experiment, wall clutters cover the range from 0 m to 2 m, and strong clutters backscattered from the sundries appear in range around 5 m. The targets echoes are masked by the strong clutters. The clutter suppression result employing EABS is shown in Fig. 8b), and all the three targets are clearly indicated. Unfortunately the residual wall clutters in range 0.5 m are stronger than Target A, and the residual sundries

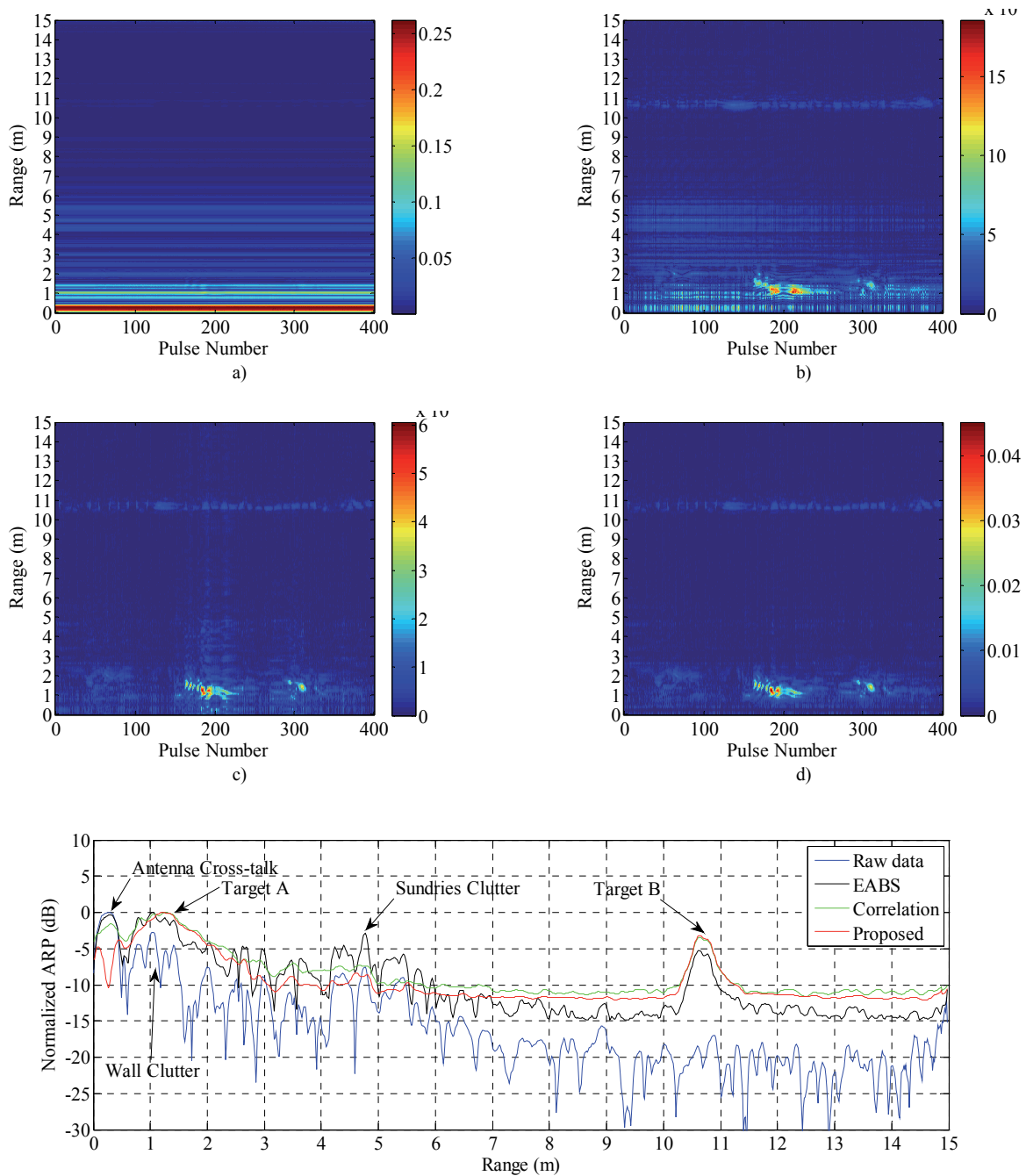


Fig. 9. The radar is setup in front of wall with a standoff distance of 1m to sense the scene with two human targets behind wall in different ranges. The organization of this figure is exactly the same as that of Fig. 7.

clutters are also comparable with Target C. However, obviously in Fig. 8c) and d), with timing jitter compensation, both the correlation and proposed methods succeed in removing the wall clutters and sundries clutters and simultaneously indicating all the three human targets. As we can observe from the four ARP distributions plotted in Fig. 8e), employing all the three methods, Target B achieves about 5 dB higher than the adjacent cell ranges level. But compared with the ARP of the raw data, EABS makes little improvement on mitigating wall clutters and the level of the wall clutters is the highest. Although the indication results of the correlation and proposed methods in Fig. 8c) and d) are similar, comparison of their ARP distributions shows that the proposed method suppresses the wall clutters to the level 6 dB below Target A and B while the correlation method only gets 3 dB. As to Target C, the proposed method achieves 4 dB higher than the sundries clutters, while EABS and correlation only obtains 1 dB and 2 dB respectively. Obviously, the proposed method obtains a higher dynamic range, which is more favorable to target detection.

Target	A	B	C
Movement	Standing still	Standing with arm swinging	Standing still
Range	1.0 m	3.0 m	6.0 m

Tab. 2. Motion states of human targets in the second experiment.

5.3 Radar with a Standoff Distance

Finally, in the third case, the radar is setup in front of wall with a standoff distance of 1 m to illustrate the timing jitter effect on the antenna cross-talk. Two human targets locate in different ranges behind wall, and their motion states are described in Tab. 3.

Target	A	B
Movement	Standing with twisting irregularly	Marking time
Range	1.0 m	10.0 m

Tab. 3. Motion states of human targets in the third experiment.

Target A stands close to the wall. We can observe from the raw data range profiles in Fig. 9a), the antenna cross-talk — the strongest echoes appear in the range of 0-0.5 m, wall direct waves and clutters are in the range of 0.5-2 m, Target A is invisible, and so is Target B. As displayed in Fig. 9b), the two targets are indicated by EABS, but residual clutters including the antenna cross-talk, wall clutters and sundries clutters are fairly strong. Again, the correlation and the proposed method succeed in removing whether the cross-talk or the wall clutters or the sundries clutters in Fig. 9c) and d), respectively. However, the correlation method yields more residuals than the proposed method. We can find from the ARP distributions provided in Fig. 9e) that the antenna cross-talk residuals in the EABS result are still compete with Target A. By contrast, the proposed method not only distinguishes Target A from the wall clutters, but also suppresses the antenna cross-talk to 5 dB below the level of Target A, while the correlation method only obtains 2 dB attenuation. Considering the

sundries clutters, they are still higher than the level of Target B, in the ARP distribution of EABS. However, the proposed method achieves a best suppression, about 5 dB lower than Target B, while the correlation method only gets about 3 dB.

5.4 Discussion

From the three experiments, we can find that timing jitter exerts an adverse impact on clutter mitigation performance in the impulse TWR. Once it is compensated, whether by the correlation or proposed method, residuals from the strong clutters like antenna cross-talk, wall clutters etc. are greatly removed, and the clutter mitigation performance is significantly improved.

Dealing with the above three experimental scenarios, the performance of the correlation method is unstable, which indicates that it is somewhat sensitivity to noise, and its performance may be degraded by the accumulated misalignment error in long-time use. However, as an extension of the correlation method, the proposed method makes use of more information to compensate the timing jitter effect, enhances the ability to resist the misalignment error and thus obtains more robust results in the three experiments.

6. Conclusion

Dealing with real systems mean the presence of timing jitter, and the nanosecond pulses employed in impulse TWR make the sensitivity to timing jitter significant. Timing jitters destroy the correlation property of received signals, and degrade the performance of TWR, especially the clutter suppression. In this paper, the timing jitter effect on clutter suppression in through-wall human indication is modeled and analyzed, a criterion namely ARP contrast is proposed to evaluate the jitter level and a method based on local ARP contrast maximization is developed to compensate the timing jitter, followed by EABS to indicate human targets. Employing the impulse TWR, through-wall sensing experiments are conducted, and validate the proposed method.

Acknowledgements

This work was supported in part by the National Natural Science Foundation of China under Grant 61271441 and the research project of National University of Defense Technology under Grant CJ12-04-02.

References

- [1] BARANOSKI, E. J. Through-wall imaging: historical perspective and future directions. *Journal of the Franklin Institute*

- Engineering and Applied Mathematics*, 2008, vol. 345, no. 6, p. 556-569.
- [2] SCHEJBAL, V., BEZOUSEK, P., CERMAK, D., NEMEC, Z., FISER, O., HAJEK, M. UWB Propagation through walls. *Radioengineering*, 2006, vol. 15, no. 1, p. 17-24.
- [3] LU, B., SONG, Q., ZHOU, Z., ZHANG, X. Detection of human beings in motion behind the wall using SAR interferogram. *IEEE Geoscience and Remote Sensing Letters*, 2012, vol. 9, no. 5, p. 968 to 971.
- [4] ROVNÁKOVÁ, J., KOCUR, D. UWB sensor based localization of persons with unknown motion activity. In *14th International Radar Symposium*. Dresden (Germany), 2013, p. 649 - 654.
- [5] HU, J., ZHU, G., JIN, T., ZHOU, Z. Adaptive through-wall indication of human target with different motions. *IEEE Geoscience and Remote Sensing Letters*, 2014, vol. 11, no. 5, p. 911-915.
- [6] ZETIK, R., CRABBE, S., KRAJNAK, J., PEYERL, P., SACHS, J., THOMÁ, R. Detection and localization of persons behind obstacles using M-sequence through-the-wall radar. In *Proceedings of SPIE - Sensors, and Command, Control, Communications, and Intelligence (C3I) Technologies for Homeland Security and Homeland Defense V*. Florida (USA), 2006, vol. 6201.
- [7] URDZIK, D., KOCUR, D., ROVNAKOVA, J. Detection of multiple targets with enhancement of weak UWB radar signals for the purposes of through wall surveillance. In *10th IEEE Jubilee International Symposium on Applied Machine Intelligence and Informatics*. Herlany (Slovakia), 2012, p. 137-142.
- [8] RICHARDS, M. A. *Fundamentals of Radar Signal Processing*. New York: McGraw-Hill, 2005.
- [9] NAG, S. Y., BARNES, M. A moving target detection filter for an ultra-wideband radar. In *Proceedings of the IEEE Radar Conference*. Alabama (USA), 2003, p. 147 - 153.
- [10] LI, J., ZENG, Z. F., SUN, J. G., LIU, F. S. Through-wall detection of human being's movement by UWB radar. *IEEE Geoscience and Remote Sensing Letters*, 2012, vol. 9, no. 6, p. 1079 - 1083.
- [11] NEZIROVIC, A., YAROVOY, A. G., LIGTHART, L. P. Signal Processing for Improved Detection of Trapped Victims Using UWB Radar. *IEEE Transactions on Geoscience and Remote Sensing*, 2010, vol. 48, no. 4, p. 2005 - 2014.
- [12] XU, Y., WU, S., CHEN, C., CHEN, J., FANG, G. A novel method for automatic detection of trapped victims by ultrawideband radar. *IEEE Transactions on Geoscience and Remote Sensing*, 2012, vol. 50, no. 8, p. 3132 - 3142.
- [13] ONUNKWO, U. A. Timing jitter in ultra-wideband (UWB) systems. *Doctor's dissertation*, Georgia Institute of Technology, 2006.
- [14] LIU, T. T., WANG, C. K. A 1-4 GHz DLL based low-jitter multi-phase clock generator for low-band ultra-wideband application. In *Proceedings of the 4th IEEE Asia-Pacific Conference on Advanced System Integrated Circuits*. Fukuoka (Japan), 2004, p. 330 - 333.
- [15] LOVELACE, W. M., TOWNSEND, J. K. The effects of timing jitter and tracking on the performance of impulse radio. *IEEE Journal on Selected Areas in Communications*, 2002, vol. 20, no. 9, p. 1646 - 1651.
- [16] CHEN, C. C., ANDREWS, H. C. Target-motion-induced radar imaging. *IEEE Transactions on Aerospace and Electronic Systems*, 1980, vol. AES-16, no. 1, p. 2 - 14.
- [17] HU, J., TU, X., ZHU, G., LI, Y., ZHOU, Z. Coupling suppression in human target detection via impulse through wall radar. In *14th International Radar Symposium*. Dresden (Germany), 2013, p. 1008 - 1012.
- [18] HU, J., ZHU, G., JIN, T., WANG, L., ZHOU, Z. Study on timing jitter in clutter mitigation of through-wall human indication. In *2013 IEEE International Conference on Ultra-Wideband*. Sydney (Australia), 2013, p. 211 - 214.
- [19] LYONS, R. G. *Understanding Digital Signal Processing*. 3rd ed. New Jersey: Prentice Hall, 2010.
- [20] HE, F., ZHU, G., HUANG, X., MOU, M., ZHOU, Z., FAN, C. Preliminary results of ultra-wideband through-the-wall life-detecting radar. In *2010 IEEE Radar Conference*. Washington DC (USA), 2010, p. 1327 - 1330.
- [21] BARRIE, G. *UWB Impulse Radar Characterization and Processing Techniques*. Technical Report, Defense R&D Canada - Ottawa, 2004.
- [22] IMMOREEV, I. I., FEDOTOV, P. G. S. D. Detection of UWB signals reflected from complex targets. In *IEEE Conference on Ultra Wideband Systems and Technologies*. Baltimore (USA), 2002, p. 193-196.
- [23] SHINAGAWA, M., AKAZAWA, Y., WAKIMOTO, T. Jitter analysis of high-speed sampling systems. *IEEE Journal of Solid-State Circuits*, 1990, vol. 25, no. 1, p. 220 - 224.
- [24] ZHU, D. Y., WANG, L., YU, Y. S., TAO, Q. N., ZHU, Z. D. Robust ISAR range alignment via minimizing the entropy of the average range profile. *IEEE Geoscience and Remote Sensing Letters*, 2009, vol. 6, no. 2, p. 204 - 208.

About Authors ...

Guofu ZHU was born in Henan, P. R. China. He received his M.Sc. and Ph.D. degrees in Information and Communication Engineering from the National University of Defense Technology in 1997, and 2001, respectively. He is currently an associated professor of the National University of Defense Technology. His research interests mainly include ultra-wideband system, radar imaging and target detection.

Jun HU was born in Henan, P. R. China. He received his M.Sc. from the National University of Defense Technology in 2010. He is currently pursuing the Ph.D. degree in the National University of Defense Technology. His main research interests include ultra-wideband radar, automatic target detection, and signal processing.

Tian JIN was born in Hubei, P. R. China. He received the M.Sc., and Ph.D. degrees in Information and Communication Engineering from the National University of Defense Technology in 2003, and 2007, respectively. He is currently an Associate Professor with the National University of Defense Technology. His fields of interest include radar imaging, automatic target detection, and machine learning.

Zhimin ZHOU was born in Shandong, P. R. China. He received the M.Sc. and Ph.D. degrees from the National University of Defense Technology in 1989 and 2002, respectively. He is currently a professor of the National University of Defense Technology. Dr. Zhou is a senior member of the Chinese Institute of Electronics. His fields of interest include ultra-wideband radar system and real-time signal processing.